

Tailored UV-laser source for fluorescence spectroscopy of biomolecules

M. Tiihonen*, V. Pasiskevicius, F. Laurell

Department of Physics, Roslagstullsbacken 21, 106 91 Stockholm, Sweden

Available online 4 August 2006

Abstract

A dual-wavelength UV-laser source was developed for biosensing. First, a passively Q-switched diode-pumped Nd:YAG laser was constructed. The astigmatic diode output beam was converted into a homogenous beam profile by utilizing a mode converter. As a result, a frequency-doubling conversion efficiency of 50% was achieved in a periodically poled KTiOPO₄. With a repetition rate of 100 Hz, the pulse energies and lengths were 650 μJ and 1.8 ns, respectively, at 532 nm with a M^2 of 1.3. The UV-generation is based on cascaded parametric processes using an intra-cavity sum-frequency mixing scheme in a periodically poled KTiOPO₄ parametric oscillator pumped at 532 nm. Here, the wavelengths 293 and 343 nm were generated, with conversion efficiencies of 7% and 6.5%, respectively, in respect to 532 nm. With pulse length 1 ns and an average power above 2.7 mW, the wavelengths were used for fluorescence measurements of non-pathogenic bacteria.

© 2006 Elsevier Ltd. All rights reserved.

Keywords: Diode pump solid-state laser; Beam transformation; Beam shaping; Optical parametric oscillator; Parametric devices; Ultraviolet generation

Pulsed ultraviolet (UV) lasers are very attractive for many applications both in science and industry, such as photo-lithography, micromachining of electronic devices and laser-induced fluorescence (LIF) spectroscopy. In order to meet the increasing demands for national security, the latter field is of great interest for detection and characterization of biological agents. The UV-excitation is targeted at the proteins or more explicitly at the aromatic amino acids, particularly tryptophan (Trp) and tyrosine (Tyr) [1], and also nucleotides such as NADH, which are involved in the cell metabolism [2]. These biomolecules have strong absorption bands in the spectral region ranging from 280 to 340 nm and emitting in the 300–600 nm region. Two or more absorption wavelengths with corresponding emission spectra are ideally used to discriminate one biomolecule from another. Preferably, when exciting an agent, the excitation wavelengths should be chosen so that the absorption spectra of the present biomolecules within the agent do not overlap. This will enable a good selectivity and classification of the agent in a rapid way.

Commonly used UV-light sources for fluorescence spectroscopy, such as xenon and tungsten–halogen arc-

lamps, suffer from poor spectral quality and require sophisticated optics to constrict the bandwidth to a narrow linewidth. More recently AlGaIn-based LEDs, which emit below 300 nm, have been developed [3]. Unfortunately, they have low output powers and limited lifetime, due to high aluminum concentration, and has a continuous spectrum far down in the visible region which can interfere with the fluorescence spectrum. Furthermore, solid-state lasers are also widely used, for e.g., Ti:sapphire (multiphoton) [1] and quadrupled or tripled Nd:YAG lasers [4,5]. However, both of these are out of the desired wavelength range. In contrast, novel solid-state lasers such as Ce:LiSAF [6] and Ce:LiCAF [7], which have continuous tuning from 280 to 315 nm, utilize a complicated pumping arrangement. A common problem is that the crystals suffer from growth defects that degrade the efficiency of the laser and thus only research samples are available at the moment. In summary, there are no compact UV-laser sources enabling emission of two or more separate wavelengths in the specified spectral region with good spectral resolution, short pulse length and good spatial beam quality. The UV laser does not need to be continuously tuneable, since the absorption bands of biomolecules are inherently broad [2]; it should rather be step-wise tuneable over the specified spectral region. An

*Corresponding author. Tel.: +46 8 5537 8148; fax: +46 8 5537 8216.

E-mail address: mt@laserphysics.kth.se (M. Tiihonen).

efficient way to obtain dual or multi-wavelength UV sources in a compact and simple design is to begin with a high-energy pulsed IR laser and then frequency convert it to UV. An attractive approach to generate tailored wavelengths is to use quasi-phased matched (QPM) materials in an optical parametric oscillator (OPO) pumped by a solid-state laser. The advantages of nanosecond OPOs over, for e.g., optical parametric generators (OPGs), under the same pump conditions are that they are more efficient, have lower thresholds and high intra-cavity intensity. In addition, it is easy to deploy wavelength tuning by changing the temperature [8], rotating the crystal [9,10], or pumping a crystal containing multiple QPM gratings [11]. The inherent high intra-cavity intensity of the OPO can be used for intra-cavity sum-frequency mixing (SFM) [12]. Utilizing the generated signal from the OPO together with the pump, it is possible to reach the desired UV range specified above.

In this work, we deployed a periodically poled KTiOPO_4 (PPKTP) parametric oscillator with intra-cavity SFM in a BBO crystal. By tailoring the QPM period in the PPKTP, the spectral range from 285 to 340 nm is accessible through SFM between the generated OPO signal and the pump. The developed dual-wavelength UV laser was used for fluorescence sensing of *Bacillus thuringiensis* (BT) stabilized in aqueous NaCl solutions. The technology opens up the possibility to assemble compact and robust instruments for rapid detection in field trails.

A diode-pumped passively Q-switched Nd:YAG laser was constructed to be used as the pump source for the parametric processes. The Nd:YAG pump module consists of a fast-axis collimated quasi-CW single broad-strip diode-laser (emitting area $1\ \mu\text{m} \times 10\ \text{mm}$), two cylindrical lenses at right angles with focal lengths $f_{\text{fast axis}} = 50\ \text{mm}$ and $f_{\text{slow axis}} = 30\ \text{mm}$, a 16.6 mm-thick biconvex cylindrical lens with radius of curvature of 5 mm (also called beam twister), and a spherical lens, $f_1 = 10\ \text{mm}$, depicted in Fig. 1. The two cylindrical lenses and the beam twister were used to transform the highly astigmatic diode beam into a homogeneous irradiance profile. In optical beam analysis of laser resonators the Hermite–Gaussian mode functions are commonly used to describe propagation through the optical system, since in real lasers the beam is

usually distorted by optical elements in the cavity, and a rectangular coordinate system is preferred because of its ability to describe both astigmatic and stigmatic beams [13]. It has been proven, both theoretically and experimentally, that astigmatic beams mathematically described by Hermite–Gaussian mode functions, such as the output from a broad-strip diode-laser, can be transformed into Laguerre–Gaussian beams by using two cylindrical lenses with the same focal length [14,15]. This, however, can only be achieved when predefined conditions are met. First, the transverse beam waists should coincide between the cylindrical lenses, which are rotated at an angle of $\pm 45^\circ$ around the propagation axis. Secondly, the focal length of the lenses should be related to the Rayleigh lengths, z_{Rx} and z_{Ry} , as $1/f = d/(z_{\text{Rx}}^2 + d^2) - d/(z_{\text{Ry}}^2 + d^2)$ [14], where $2d$ is the distance between the cylindrical lenses. Third, the lenses should be positioned where the two transverse radii of the astigmatic beam are equal. However, all of these conditions are difficult to meet when beam-shaping a broad-strip diode-laser, since the beam quality parameters (M^2) are highly different for the slow and fast axis. Nevertheless, it is still possible to equalize the beam quality parameters in the x - and y -axes (slow axis (SA) and fast axis (FA)) so that a homogenous beam profile is obtained. In our set-up, instead of using two cylindrical lenses a thick cylindrical lens is used as a mode converter. The extension between the two cylindrical surfaces (called the center plate) is determined by [16]

$$t = \frac{2r}{n-1} \left(1 + n \frac{1-\sqrt{2}}{\sqrt{2}} \right), \quad (1)$$

where n is the refractive index (SF4 glass, $n = 1.755$) and r is the radius of curvature. Thus the total length, L , is then $L = t + 2r = 16.6\ \text{mm}$. With the two cylindrical lenses 5 mm apart, f_{FA} and f_{SA} focused the FA and SA, respectively, to a coinciding focus within the beam twister, which was rotated at an angle of $\alpha = 45^\circ$. The measured beam waists were $\omega_{\text{FA}} \approx 200\ \mu\text{m}$ and $\omega_{\text{SA}} \approx 270\ \mu\text{m}$, respectively, whereas the Rayleigh length for the FA was much longer than for the SA, $z_{\text{R,FA}} \gg z_{\text{R,SA}}$. The imperfect mode matching resulted in a diamond-shaped output beam with equally diverging transverse components, a so-called

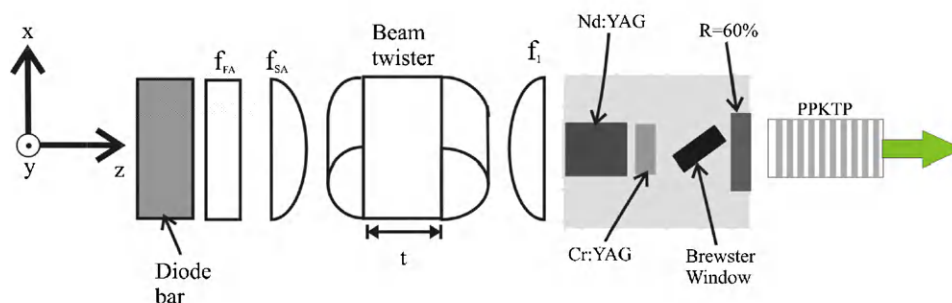


Fig. 1. The diode pumped passively Q-switched Nd:YAG laser, with beam twisting optics. The total length of the laser is 25 cm.

twisted Hermite–Gaussian beam with complex arguments [15]. The nearly symmetric beam was focused with a lens, f_1 , to a beam radius of 1 mm (e^{-2} intensity) inside the laser medium.

The Nd:YAG crystal was 4 mm long with a diameter of 5 mm and it had a doping concentration of 1.1% atm. It was highly reflective on one side and AR-coated on the other side at 1064 nm and AR-coated on both sides at the 808 nm pump wavelength. It was contacted with indium foil to a cylindrical copper holder, which was air-cooled. Pulsed operation was provided with a Cr:YAG saturable absorber, with an initial transmission of 34%. To ensure vertical polarization, a Brewster window was inserted between the Cr:YAG crystal and the output mirror. This mirror had a reflectivity of 60% at the signal wavelength. The laser generated pulses of 2.3 ns (FWHM) at 100 Hz repetition rate and an average power of 130 mW, with an optical-to-optical efficiency of nearly 10%. The beam-quality parameter, M^2 , and beam radius at the output was measured as 1.3 and 390 μm (e^{-2} intensity), respectively. In front of the laser cavity, a 3-mm-long PPKTP crystal with a period of $\Lambda = 9.01 \mu\text{m}$ generated second harmonic radiation at 532 nm. It was placed on a copper holder that held a temperature of 22 °C and was AR-coated at 1064 and 532 nm. A 50% optical conversion efficiency was measured and a shortening of the pulse to 1.8 ns was observed, while the M^2 -value remained the same. The pulse shortening is a consequence of the second-order non-linear process, which is proportional to the square of the electric field and hence strongest around the peak of the laser pulse. The laser cavity and the doubling crystal were mounted on a monolithic copper block with a length of 35 mm. The total length of the laser, including diode bar, beam twisting and focusing optics, and PPKTP crystal was 25 cm.

Two singly resonant OPOs with intra-cavity SFM were constructed. They are similar in design, but generating different wavelengths. Both consisted of an incoupling mirror, a PPKTP crystal, a Type I (ooe) BBO crystal, a dichroic mirror at an angle of 45° to the cavity, and a low-transmission mirror closing the cavity. The cavity design is depicted in Fig. 2. The incoupling mirrors were highly reflective (HR), $R_S \approx 98\%$, at the signal wavelengths and transmitted approximately to 95% of the pump. The generated signal wavelength from the PPKTP was tailored following the phase-matching conditions:

$$\Delta k = k_p - k_s - k_i - 2\pi/\Lambda, \quad (2)$$

where k_p , k_s and k_i are the wave vectors of the pump, the signal and the idler, respectively and Λ the grating period. The wavelengths from 615 to 940 nm can be accessed by changing the grating period from 14.13 to 9.1 μm and with consecutive SFM the spectral range of 285–340 nm can be reached. Here, the QPM periods $\Lambda_{650} = 12.77 \mu\text{m}$ [17] and $\Lambda_{940} = 9.1 \mu\text{m}$ [10] were chosen in order to generate 650 and 940 nm, respectively. The PPKTP samples were 8 mm long, 5 mm wide and 1 mm thick and were AR-coated for the signal, the pump and the idler. Furthermore, the 5 mm-

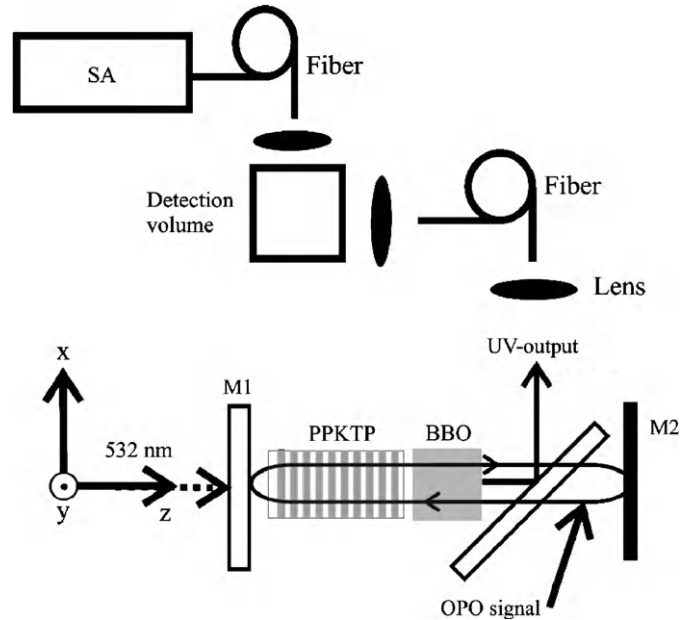


Fig. 2. The PPKTP parametric oscillator with intracavity SFM. The signal was resonated inside the cavity, and SFM together with the non-depleted pump. The UV radiation was coupled out by the dichroic mirror and then coupled into a fiber. The UV is then launched into the detection volume and the fluorescent spectrum is recorded with the spectrum analyzer (SA). It is the same coordinate system as in Fig. 1.

long AR-coated BBO crystals were cut and polished at the angles $\theta_1 = 42.1^\circ$ and $\theta_2 = 33.4^\circ$, respectively, to the crystallographic c -axis. They generated the UV wavelengths 293 and 343 nm, respectively, in SFM between the signals and the pump. The dichroic mirrors coupled out the generated UV wavelengths and had a reflectivity of $\sim 95\%$ at 293 and 349 nm, respectively, while transmitting the signal and the pump wavelengths. Finally, the output mirrors were AR-coated for the pump and the idler, while reflecting $\sim 80\%$ of the signals to keep the intra-cavity intensities below the damage threshold for the coatings. The entire OPO-SFM cavity was 26 mm long. The 532 nm pump beam was focused to a radius of 200 μm (e^{-2} intensity) within the PPKTP OPO crystal, utilizing a telescope consisting of two lenses, $f_2 = 50 \text{ mm}$ and $f_3 = -75 \text{ mm}$, separated 20 mm apart and 50 mm from the second-harmonic-generating PPKTP crystal.

First the OPOs were characterized individually, without BBO crystals, in a 20 mm-long cavity. In both cases, the output mirrors had a reflectivity of 80% at the signal wavelengths. The measured thresholds were 20 and 81 μJ , respectively, for the PPKTPs mentioned above. The signal powers varied linearly with the pump power and at 44 mW the signal pulse energies were 132 and 80 μJ , respectively. The latter was calculated through the Manley–Rowe relation [18], since the OPO was operated close to degeneracy. At this point the idler at 1225 nm and the signal at 940 nm could not be separated. In contrast, the former OPO's idler wave at 2930 nm was mainly absorbed in the BK7 glass and could be neglected. Furthermore, the

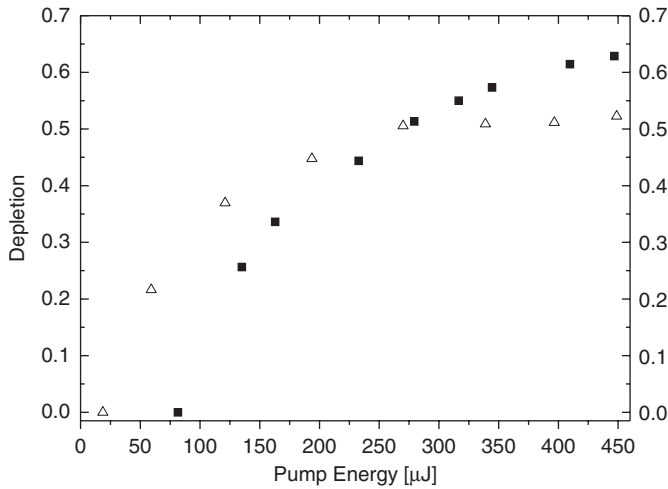


Fig. 3. The depletion versus pump energy. The 650 nm OPO reached 52% depletion at maximum pump power (open triangles), while the 940 nm OPO attained 63% at the same level (filled squares).

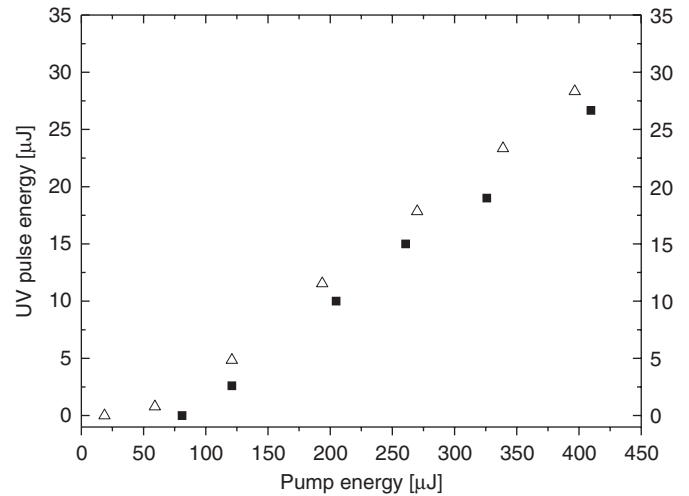


Fig. 4. UV radiation as a function of 532 nm pump energy. Pulse energies of 32 μJ at 293 nm (open triangles) and 26 μJ at 343 nm (filled squares), respectively, were obtained. The total conversion efficiencies were 3.5% and 3%, respectively.

efficiencies depicted in Fig. 3 reached values of 52% and 61%, respectively. The somewhat lower value in the former OPO was attributed to parasitic oscillation observed within the PPKTP crystal, due to poor quality of the coatings. The beam quality measurements revealed an M^2 -value of 4.5 for 650 nm, while for the 940 nm-generating OPO it was 1.8 times diffraction limited. In addition, the measured pulse widths were again shortened to ~ 1 ns (FWHM) in both OPOs. As the BBO crystals are inserted in the cavities along with the dichroic mirrors, the thresholds are to some extent increased due to longer cavity length. Nevertheless, at maximum pump power the intra-cavity SFM produced output powers of 3.2 mW at 293 nm and 2.7 mW at 340 nm. This corresponds to a conversion efficiency of 7% and 6.5%, with respect to the incident 532 nm pump, and a total conversion efficiency of 3.5% and 3% with respect to the IR. The output energies as a function of incident pump energy are shown in Fig. 4. Single-pass-pumped OPOs with intra-cavity SFM are inherently unidirectional; therefore the UV-radiation was only generated in the direction of the pump wave vector, k_p . There was no measurable difference of the pulse lengths and they were still 1 ns. The recorded spectra are shown in Fig. 5. The UV output at 293 nm reveals a narrow spectral bandwidth of approximately of 3.50 THz (FWHM), while at 343 nm the spectrum is about six times broader (20.4 THz). When moving closer to degeneracy of this PPKTP OPO (from 650 to 940 nm) the spectral bandwidth increases, and as a consequence, the 343 nm output inherits the broader spectrum of the 940 nm signal [10]. In addition, the peak at 370 nm is SFM between the idler at 1225 nm and the pump, which was filtered out when the pulse energies were measured.

For proof of concept of the developed dual-wavelength UV laser, a fluorescence detection system was constructed using a PMT-array in order to measure low concentrations. The PMT-array from Hamamatsu (model H7260-4) has 32 channels linearly spaced, and it was connected to a

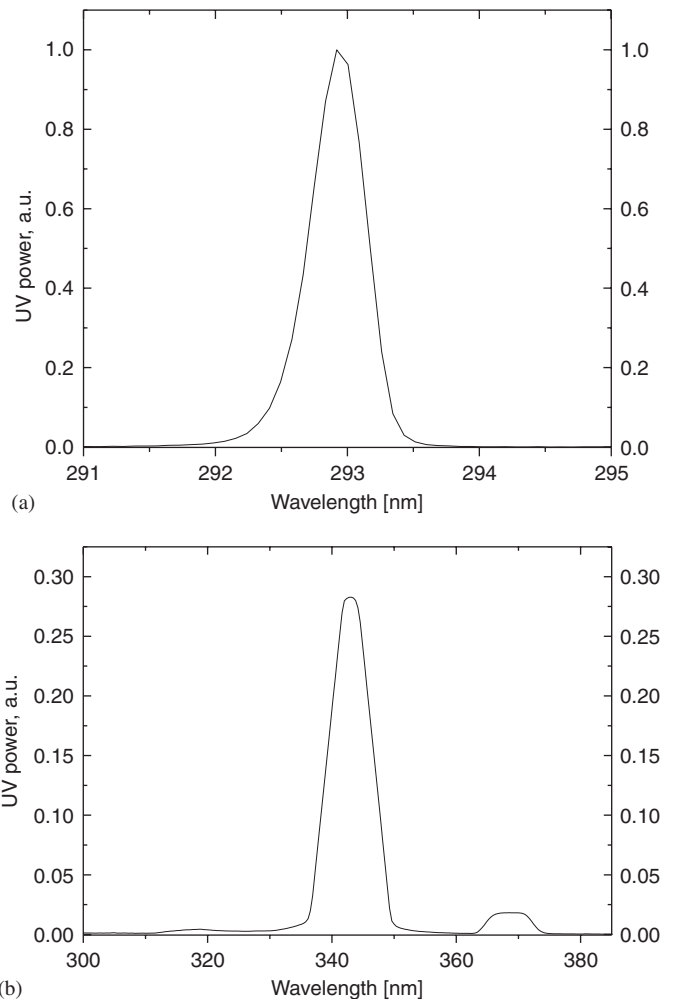


Fig. 5. (a) Output spectrum at 293 nm, recorded with an Ocean Optics USB2000 spectrometer. (b) Output spectrum at 343 nm, recorded with an Ocean Optics USB2000 spectrometer. A peak at 371 nm is attributed the parasitic generation of the idler and the pump. This was however filtered out when conducting fluorescence measurements.

spectrograph from Oriel (model 77442), with a fiber connection [19]. The UV light from the laser was coupled into a 10 m long quartz fiber, with a diameter of 1 mm and an NA of 0.39, seen in Fig. 2. The fiber throughput was measured as 1%, due to high absorption in the fiber and unoptimized in- and outcoupling. Despite the very poor transmission, the launched UV radiation was sufficient to excite the biomolecules. The BT samples were prepared by the Swedish Defense Research Agency (FOI NBC, Sweden) in a salty solution and had a concentration of 10 $\mu\text{g}/\text{ml}$. Fluorescence spectrum was recorded for both excitation wavelengths and is shown in Fig. 6. The shift in the fluorescence spectrum, when comparing excitations at 293 nm with 343 nm, is a result of different absorption bands being accessed within the bacteria. The main target for excitation at 293 nm is Trp, while NADH is the target at 343 nm [2]. However, the bacteria contain a large amount of other fluorescent biomolecules, which contributed to the emission spectrum and at this point their origin and characteristics are not known. On the other hand, this shift and most importantly the change in characteristics of the spectrum can help in the distinction between natural

occurring bacteria and biological warfare agents (BWA) by using multivariate analysis [20,21]. Unfortunately, this of kind analysis is outside the scope of this investigation. However, a more extensive study of different BWA with our developed UV source has been conducted elsewhere, see Ref. [19]. The UV laser will be used in future investigations of BWA to optimize the choice of excitation wavelengths in order to characterize different BWA.

In conclusion, we have constructed a compact UV laser with dual-wavelength outputs. The laser was operated at 100 Hz with 1 ns long pulses and pulse energies above 25 μJ at 293 and 343 nm. The laser was built around PPKTP parametric oscillator technology along with an intra-cavity SFM-scheme with an overall efficiency from IR to UV above 3%. This made the system very compact and robust and it is possible to power it with car batteries for field trails. This laser is an important and unique light source for detection systems of bioagents, and it was shown that the generated energies were good enough for fluorescence investigation of *B. thuringiensis*. The wavelength 293 nm is close to optimum for excitation of the aromatic amino acid Trp, while the auxiliary wavelength adds additional fluorescence data to facilitate the classification of bioagents. However, it is not yet determined which or how many excitation wavelengths are needed in order to conduct a definite identification. With QPM technique, the wavelength can be easily changed in the present setup and this will be further investigated. The next version of this laser will be with kHz repetition rate in order to meet the demand for faster and reliable data collecting.

We acknowledge Swedish defense Agencies (FOI, FMV and HQ) for financial support within the biological detection projects. We thank Per Jonsson, Mikael Lindgren, Torbjörn Tjärnhage at the Swedish Defence Research agency (FOI) for providing the spectrum of the BT samples. We also want to acknowledge Stefan Spiekermann and Jonas E Hellström for assisting with the beam-shaping optics.

References

- [1] Lippitz M, Erker W, Decker H, Van Holde KE, Basché T. Two-photon excitation microscopy of tryptophan containing proteins. *Proc Natl Acad Sci* 2002;99:2772–7.
- [2] Lakowicz JR. Principles of fluorescence spectroscopy. 2nd ed. New York: KA/PP; 1999.
- [3] Vitta P, Kurilcik N, Novickovas A, Jursenas S, Calkauskas H, et al. AlGaIn-based deep UV LEDs for fluorescence sensing. *Proc SPIE* 2004;5617:249–60.
- [4] Bode M, Spiekermann S, Fallnich C, Welling FH. Ultraviolet single-frequency pulses with 110 mW average power using frequency-converted passively Q-switched miniature Nd:YAG ring lasers. *Appl Phys Lett* 1998;73:714–6.
- [5] Kitano H, Matsui T, Sato K, Ushiyama N, Yoshimura M, et al. Efficient 355-nm generation in CsB₃O₅ crystal. *Opt Lett* 2003;28:263–5.

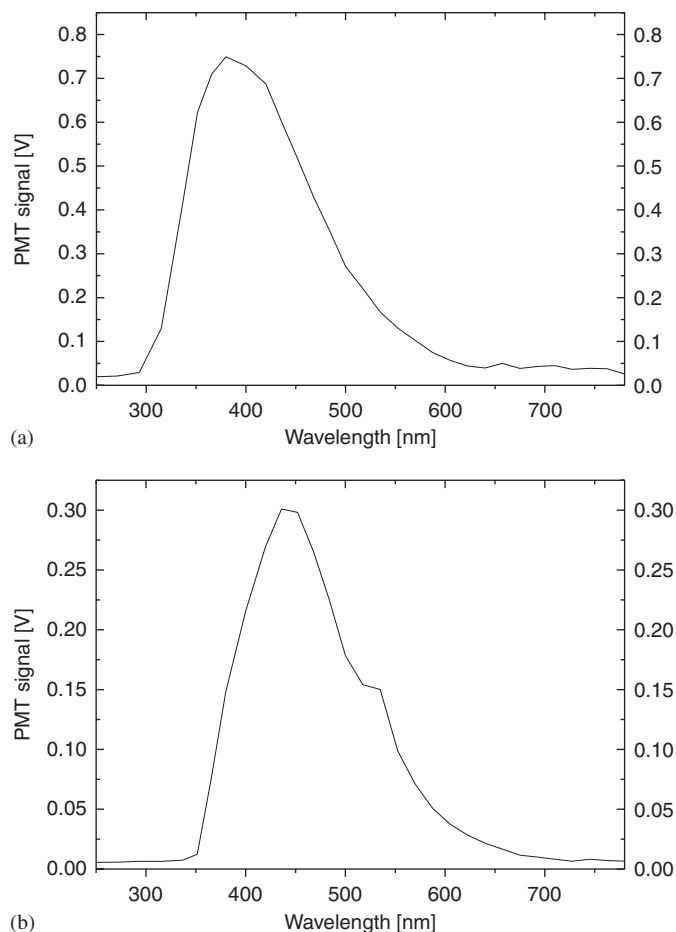


Fig. 6. (a) Recorded fluorescence spectrum at an excitation of BT at 293 nm; the sample concentration was 10 $\mu\text{g}/\text{ml}$. Measured at a gain of 1.4×10^6 for the PMT-array [19]. (b) Recorded fluorescence spectrum at an excitation of BT at 343 nm; the sample concentration was 10 $\mu\text{g}/\text{ml}$. Measured at a gain of 1.4×10^6 for the PMT-array [19].

- [6] McGonigle AJS, Coutts DW, Girard S, Moncorgé R. A 10 kHz Ce:LiSAF laser pumped by the sum-frequency-mixed output of a copper vapour laser. *Opt Commun* 2001;193:233–6.
- [7] Pinto JF, Esterowitz L, Quarles GJ. High performance Ce³⁺:LiSrAlF₆/LiCaAlF₆ UV lasers with extended tunability. *Electron Lett* 1995;31:2009–11.
- [8] Peltz M, Bader U, Borsutzky A, Wallenstein R, Hellström J, Karlsson H, et al. Optical parametric oscillators for high pulse energy and high average power operation based on large aperture periodically poled KTP and RTA. *Appl Phys B* 2001;73:663–70.
- [9] Missey MJ, Dominic V, Powers PE. Periodically poled lithium niobate monolithic nanosecond optical parametric oscillators and generators. *Opt Lett* 1999;24:1227–9.
- [10] Tiihonen M, Pasiskevicius V, Laurell F. Spectral and spatial limiting in a idler-resonant PPKTP optical parametric oscillator. *Opt Commun* 2005;250:207–11.
- [11] Myers LE, Eckardt RC, Fejer MM, Byer RL, Bosenberg WR. Multigrating quasi-phase-matched optical parametric oscillator in periodically poled LiNbO₃. *Opt Lett* 1996;21:591–3.
- [12] Fix A, Ehret G. Intracavity frequency mixing in pulsed optical parametric oscillators for the efficient generation of continuously tunable ultraviolet radiation. *Appl Phys B* 1998;67:331–8.
- [13] Siegman AE. *Lasers*, 1st ed. University Science Books; 1986.
- [14] Beijersbergen MW, Allen L, van der Veen HELO, Woerdman JP. Astigmatic laser mode converters and transfer of orbital angular momentum. *Opt Commun* 1993;96:123–32.
- [15] Laabs H, Gao C, Weber H. Twisting of three-dimensional Hermite–Gaussian beams. *J Mod Opt* 1999;46:709–19.
- [16] Laabs H, Gao C, Weber H, Kugler N, Shao C. Transformation of Hermite–Gaussian-beams into complex Hermite–Gaussian and Laguerre–Gaussian beams. *Proc SPIE* 1999;3611:258–68.
- [17] Pasiskevicius V, Karlsson H, Laurell F, Butkus R, Smilgevičius V, Piskarskas A. High-efficiency parametric oscillation and spectral control in the red spectral region with periodically poled KTiOPO₄. *Opt Lett* 2001;26:710–2.
- [18] Sutherland RL. *Handbook of nonlinear optics*, 1st ed. New York: Marcel Dekker Inc.; 1996.
- [19] Jonsson P, Kullander F, Nordstrand M, Tjärnhage T, Wästerby P, Lindgren M. Development of fluorescence-based point detector for biological sensing. *Proc SPIE* 2004;5617:61–74.
- [20] Qu JY, Chang H. Fluorescence spectral imaging for characterization of tissue based on multivariate statistical analysis. *J Opt Soc Am A* 2002;19:1823–31.
- [21] Tjärnhage T, Strömqvist, Olofsson G, Squirell D, Burke J, et al. Multivariate data analysis of fluorescence signals from biological aerosols. *Field Anal Chem Technol* 1999;3:221–39.